INORGANIC CHEMISTRY FRONTIERS

RESEARCH ARTICLE

View Article Online
View Journal | View Issue

Check for updates

Cite this: *Inorg. Chem. Front.*, 2025, **12**, 4449

Low-valent tantalum/gold clusters: oxidation, protonation, and C–H activation†

Michela L. Maiola and Joshua A. Buss *

Gold-based catalysts are topical heterogeneous and molecular species, the chemical diversity of which can be expanded through heterometal doping. Herein, we leverage a carbonyl-free metal–metal salt metathesis protocol to access rare examples of low-valent tantalum/gold multimetallics. The initial reaction between $[Ta(naphthalene)_3]^-$ and gold(I) synthons affords a trimetallic monohydride cluster (**2**). Whereas dihydrogen addition to **2** results in deauration *en route* to a Ta–μH_2–Au complex (**1**), oxidative transformations—either addition of chemical oxidants or cluster protonation—conserve the trimetallic core, even in the absence of a polynucleating ligand. The resultant series of compounds provides experimental anchors for computational interrogation of polarized metal–metal interactions as a function of metal identity, formal oxidation state, and ligand sphere. The electronic structure of these clusters showcases significant Ta–arene covalency, even at higher oxidation states, rationalizing a recalcitrance to undergo ligand substitution. Furthermore, the addition of *in situ* generated Au^+ to **2** results in an arene C–H activation process, highlighting that the naphthalene ligands in these complexes are simultaneously substitutionally inert and prone to functionalization.

Received 3rd February 2025,
Accepted 2nd April 2025

DOI: 10.1039/d5qi00334b

rsc.li/frontiers-inorganic

Introduction

The synthesis of heterometallic gold clusters flourished in the 1980s,[1,2] during which time their relevance to surface catalysis was emphasized as the so-called cluster-surface analogy gained prominence.[3,4] Synthetically, many of these species were accessed *via* addition of Au(I) precursors to existing clusters or *via* salt-metatheses with polycarbonyl metallates (Fig. 1A).[2,5–15] In spite of the diversity of cluster architectures accessed in this way, the thermal reactivity of the resultant species is markedly distinct from that of heterogeneous active sites.[16–18] Contrasting the latter, in which highly reactive, coordinatively unsaturated fragments are responsible for substrate binding and activation,[19,20] the carbonyl ligands commonly found in low-valent molecular systems stunt their reactivity *via* electronic attenuation and coordinative saturation.[17] Focus therefore shifted to using these platforms to explore the electronic structure of metal–metal bonding and the impact of metal ion identity on bonding modes.[2,12]

Higher valent heterometallic gold fragments, particularly those bearing bridging hydride ligands, have likewise been explored as informers of electronic structure and fundamental reactivity trends relevant to higher nuclearity gold-based nanoparticles and materials.[21–36] Distinct from the preparations of low-valent clusters, these bi- and trimetallic compounds are often accessed by addition of aurous precursors bearing labile

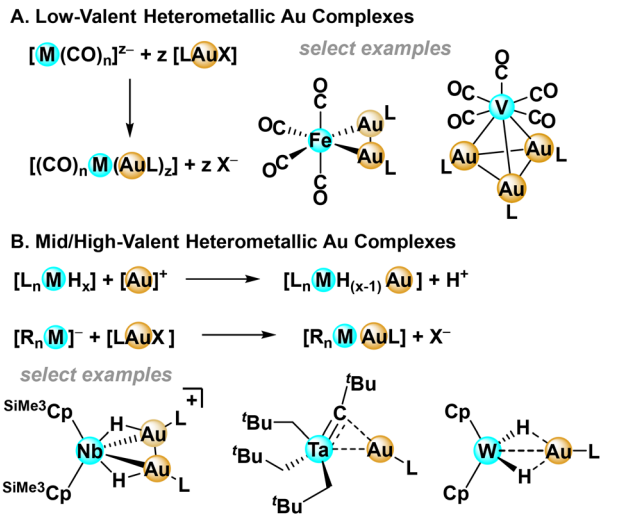

Fig. 1 Established synthetic routes to heterometallic gold coordination complexes. Low-valent mixed-metal gold complexes are generally accessed *via* salt-metatheses with transition metal polycarbonyls (A). High-valent M/Au compounds are routinely prepared *via* treatment of hydride or alkyl complexes with appropriate gold(I) precursors (B).

Willard Henry Dow Laboratory, Department of Chemistry, University of Michigan, 930 N. University Avenue, Ann Arbor, MI 48109, USA. E-mail: jbuss@umich.edu

†Electronic supplementary information (ESI) available: Synthetic and computational details; spectral data. CCDC 2409547–2409550, 2432513 and 2432514. For ESI and crystallographic data in CIF or other electronic format see DOI: https://doi.org/10.1039/d5qi00334b

or strongly Brønsted-basic ligands (Fig. 1B).[21,24,26,29,31–36] This strategy is effective for the generation of mid- to high-oxidation state complexes that often feature bridging hydride ligands. Quite recently, Camp and coworkers disclosed a salt-metathesis synthesis of Ta(v)/Au(i) complexes bridged by unsaturated Ta–C bonds, in which bimetallic cooperativity enables unusual ketenyl formation *via* deoxygenation of CO_2.[22] There is a scarcity of literature, however, disclosing low-valent early–late heteromultimetallic species, compounds with formal valencies that more accurately mirror a heterogeneous surface.

In heterogeneous catalysis, the multicomponent reactivity of either gold and a non-innocent support or heterometallic gold catalysts is well-established.[37,38] These effects are particularly important for imparting gold with atypical reactivity.[39–41] Hydrogen spillover—the exchange of surface hydrogen atoms between metals or between gold and a support—is a critical mechanistic phenomenon leveraging bimetallic or metal/support cooperativity.[42–47] Both the intrinsic metal–metal interactions and their influence on the electronic structure of bridging hydride ligands is central to understanding this process, a key step toward the rational design and implementation of improved heterometallic catalysts that coordination chemistry is uniquely suited to address.[28,48]

In line with our group's interest in using well-defined molecular clusters as models of surface active sites,[49,50] we recently reported an enabling synthetic methodology for the formation of early–late heterobimetallics.[51] Our approach addressed a longstanding challenge in bottom-up mixed-metal cluster synthesis, facilitating a rational, stepwise increase in cluster nuclearity and providing access to a series of bi-, tri-, and tetrametallic carbene-supported Ta/Cu compounds (Fig. 2A).

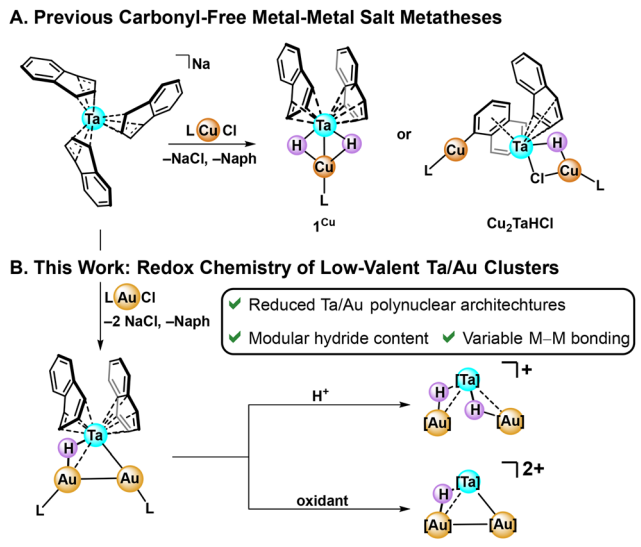

Fig. 2 Synthesis of early–late heterometallic hydride complexes *via* carbonyl-free metal–metal salt metathesis. Our prior disclosure investigated the metathesis, hydride origination, and reductive chemistry of Ta/Cu compositions (A). This work expands the chemistry to gold, showcasing the effect of oxidation and protonation state on metal–metal bonding (B).

Herein, we expand the scope of the carbonyl-free metal–metal salt metathesis to include the synthesis of carbene-supported heteromultimetallic gold clusters. Taking advantage of the more accessible redox properties of gold, we demonstrate oxidation and protonation chemistry, subsequently targeting naphthalene substitution (Fig. 2B). Contrasting analogous reaction conditions with copper, the major product of the initial salt metathesis reaction is a $TaAu_2$ trimetallic species featuring unsupported Au–Au and Au–Ta bonds. Redox chemistry, informed by cyclic voltammetry studies, generates two novel Ta/Au clusters. Both single crystal X-ray diffraction (SCXRD) and density functional theory (DFT) studies provide structural and electronic comparisons across Ta/Au trimetallics, highlighting changes in metal–metal bonding as a function of ligation and redox state. This work showcases the versatility of the salt metathesis strategy for rationally accessing rare low-valent mixed-metal complexes absent electronically deactivating, strongly π-acidic carbonyls.

Results and discussion

Ta/Au mixed-metal cluster synthesis and reactivity

Building on our previous work, Ellis' tris(naphthalene) tantalate ($[Ta(naph)_3]^-$)[52] was treated with one equivalent of cyclic (alkyl)(amino)carbene gold chloride (^{Et}CAACAuCl)[53] in dimethoxyethane (DME). Distinct from the analogous reaction with carbene-supported cuprous salts, the initial metathesis produced a mixture of bimetallic (^{Et}CAACAu)H_2Ta(naph)$_2$ (**1**) and trimetallic (^{Et}CAACAu)$_2$HTa(naph)$_2$ (**2**) complexes in 13% and 30% yield, respectively (Fig. 3A). The incorporation of hydride ligands during the salt metathesis reaction aligns with our findings from the Ta/Cu chemistry, where detailed isotopic labeling experiments showed that the hydride ligands were sourced from both naphthalene and solvent during the formation of the bis(μH) diamond core.[54] Compounds **1** and **2** can be separated based on differential solubility, with the former readily dissolving in aliphatic solvents.

The bimetallic complex **1**, best described as a Ta^IAu^I species, was fully characterized *via* nuclear magnetic resonance (NMR) spectroscopy and SCXRD. The ^{1}H NMR spectrum of **1** reveals a mixture of both a symmetric (C_{2v}) major species ($\delta_{\mu H}$ = −2.78 ppm) and an asymmetric (C_s) minor species ($\delta_{\mu H}$ = −1.48 ppm), assigned to coordination isomers with *syn*- and *anti*-naphthalene rings, respectively. This structural phenomenon was likewise observed for the copper congeners, in which the proportion of the *anti*-isomer correlated inversely with the steric profile of the carbene ligand. For **1**, the *anti*-isomer is favored more so than in the isostructural copper analog (34% *vs.* 22%), consistent with the larger radius of Au. Despite being the minor species in solution, complex **1** preferentially crystalizes in an *anti*-naphthalene conformation. SCXRD analysis reveals a Ta–Au distance of 2.8536(2) Å, longer than the only previously reported low-valent Ta–Au contact (2.7202(2) Å),[55] but decidedly shorter than a recently disclosed alkylidyne-supported Ta–Au separation (2.9462(3) Å).[22] The formal shortness

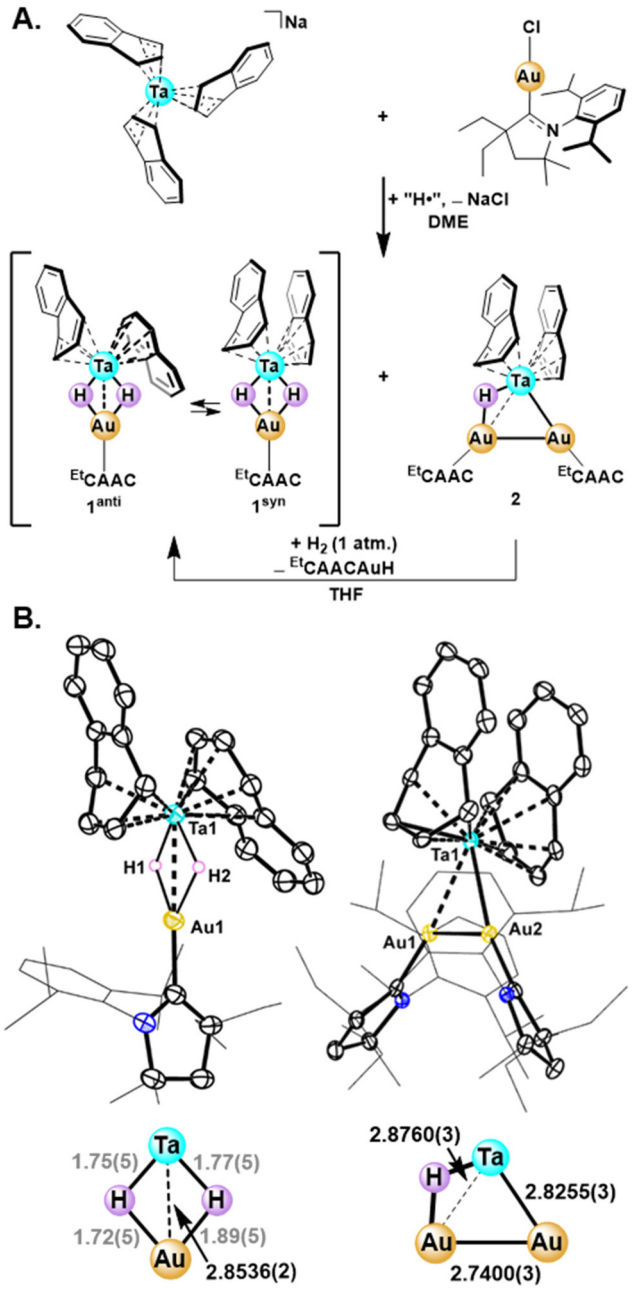

Fig. 3 Synthetic pathway to (A) and solid-state structures of (B) mixed Ta/Au bi- and trimetallic hydride complexes. SCXRD structures are shown with thermal anisotropic displacement ellipsoids at a 50% probability level and non-hydride H atoms omitted for clarity. The hydride H-atoms in **1** were resolved in the Fourier map; their locations were refined freely and their U_{iso} values were treated with a riding model. Bond metrics for the bimetallic cores are reported in Å.

ratio (FSR)[56] of the Ta–Au contact (1.05) resides on the upper range of a covalent single bond, reflecting the key role the hydrides play in stabilizing the heterobimetallic core (*vide infra*).

The structure of **2** was likewise interrogated *via* a combination of solution spectroscopy and SCXRD.[57] The ^{1}H NMR spectrum displays broad, but diamagnetic, resonances at 5.83, 4.79 and 3.12 ppm, accounting for sixteen protons of the Ta-bound naphthyl rings. The presence of a single hydride was supported by a broad high-field singlet at −1.79 ppm (THF-d_8, 25 °C) with a relative integration of one. The breadth of these signals is attributed to a ring slip isomerization process—interconversion of *syn*- and *anti*-conformations—that is intermediate on the NMR timescale at room temperature. Cooling the sample to −80 °C, the hydride singlet sharpens (Δ_{FWHM} = 106 Hz at 25 °C *vs.* Δ_{FWHM} = 16 Hz at −80 °C), and the three naphthalene peaks split into sixteen distinct signals with relative integrations of one proton each, supporting this hypothesis (Fig. S25†). Notably, the hydride chemical shift (PhMe-d_8, −80 °C: δ = −1.29 ppm) is similar to that of the related μH motif in $\mathbf{1}^{anti}$, which, in combination with the inferred C_1 symmetry, suggests that the *anti*-isomer of **2** is thermodynamically preferred in solution. Even so, trimetallic **2** crystallizes with a *syn*-naphthalene geometry, featuring both supported (Ta1–Au1: 2.8760(3) Å) and unsupported (Ta1–Au2: 2.8255(3) Å) mixed-metal bonds (Fig. 3B). The hydride ligand in **2** was not discernable in the Fourier map; however, the combined structural and spectroscopic data, particularly the orientation of the naphthyl rings, are consistent with a Ta1–μH–Au1 structure. A more in-depth discussion precluding alternative structures is presented in the ESI.† The naphthyl rings are rotated 60.66(5) degrees relative to the M_3 centroid, biasing the cluster edge featuring the unsupported Ta–Au bond. The Au1–Au2 distance of 2.7400(3) Å is significantly shorter than a related heterotrimetallic cluster generated from salt metatheses between Collman's reagent $[Fe(CO)_4]^{2-}$ and PPh_3AuCl (*cf.* 2.93 Å)[15] and is very similar to the Au–Au distance in a previously reported Au_2Nb complex (2.736 Å),[35] which bears a formal Au–Au bond. This coinage metal–coinage metal bond is a notable difference in the salt metathesis chemistry of copper and gold. The former generates a trimetallic complex upon reaction with $[Ta(naph)_3]^-$ with no Cu–Cu interaction, a σ-bound copper aryl, and a second copper center bridged to tantalum by both a μH and μCl (*cf.* **Cu_2TaHCl**; Fig. 2A). With gold, the trimetallic features a direct Au–Au bond, which we attribute to both the aurophilicity of gold and its more favorable reduction (relative to copper).

Early metal-doped coinage metal surfaces are of significant interest within the context of apolar bond activation. Biener and coworkers recently analyzed H/D exchange on a titanium doped Cu(111) surface through a combined experimental and computational effort.[58] This work, and others,[45,59–63] purport a mechanism in which the heterometal (*i.e.* Ti) serves as the site of H_2 activation due to its higher affinity to bind H_2 as compared to copper, which only weakly interacts with H_2. The molecularly adsorbed H-atoms are then proposed to migrate away from the active site and onto the coinage metal (*i.e.* spillover). Against this backdrop, we were keen to explore H_2 reactivity with complexes **1**, $\mathbf{1}^{Cu}$, and **2**.

Addition of 1 atm. of H_2 gas to a THF solution of complex **2** results in deauration, yielding the bimetallic dihydride **1** (Fig. 3A). This chemistry is reminiscent of the reactivity

observed between the ^{Et}CAAC-supported copper/tantalum trimetallic, **Cu_2TaHCl**, and H_2, despite the significant structural differences described above. Whereas H_2 addition (1 atm.) to **1** does not result in conversion to a new species, H/D exchange was observed when treating **1** with D_2. Room temperature addition of D_2 gas affords a mixed hydride/deuteride diamond core, **$1^{H/D}$**, which, upon heating to 45 °C, is fully deuterated within 24 hours.[64] This is in stark contrast to the copper congener, **1^{Cu}**, which shows no discernable H/D exchange, even after heating to 65 °C (Fig. S25–27†). The heightened reactivity of the tantalum/gold complexes is attributed to the decreased steric pressure around the metal centers (corroborated by the increased propensity for naphthalene isomerization) and more covalent Ta–μH–Au bonding (*vide infra*). Both of these features are envisioned to promote D_2 interaction with the low-valent Ta center in the tantalum/gold heterobimetallic. Despite the high degree of naphthalene activation, there was no evidence with either H_2 or D_2 for (partial) reduction of the Ta-bound arene rings.

Oxidation *versus* protonation

Toward our goal of substituting the naphthalene rings for surface-catalysis-relevant small molecules,[52,65] we hypothesized that a more oxidized Ta center would better facilitate naphthalene exchange and pursued cyclic voltammetry (CV) studies of both **1** and **2**. The CV of **1** showed an apparent quasi-reversible two-electron oxidative feature at −0.66 V coupled with re-reductions at −0.83 V and −2.33 V (*vs.* Fc/Fc^+; Fig. S31†). The electrochemistry of **2** displayed two overlapping quasi-reversible oxidations at −1.18 V and −1.10 V (*vs.* Fc/Fc^+; Fig. 4). Square wave voltammetry (SWV) better resolved these CV features, clearly displaying two events; however, the second oxidation event passes attenuated current as compared to the first, consistent with a chemical change occurring on the timescale of the electrochemical measurement.[66] The reductive sweep of the SWV is symmetric, with features at −1.10 V and −1.18 V (*vs.* Fc/Fc^+), suggesting no chemical changes occur during reduction. Encouraged by the apparent reversibility of the oxidation features for **2**, we explored chemical oxidations of this cluster with ferrocenium tetrakis[3,5-bis(trifluoromethyl)phenyl]borate (FcBArF).

To take advantage of diamagnetic ^{1}H NMR handles, a two-electron oxidation was targeted first. The addition of two equivalents of FcBArF to **2** in thawing DME resulted in formation of an oily, orange solid. ^{1}H NMR spectroscopy revealed chemically inequivalent naphthalene rings with a total of eight naphthyl proton peaks, each with a relative integration of two, ranging from 7.27 to 3.25 ppm. Both the ^{Et}CAAC ligand and BArF anion presented a relative integration of two, consistent with an intact, doubly oxidized trimetallic complex, $[(^{Et}CAACAu)_2HTa(naph)_2]^{2+}$ (**3**, 72% yield, Scheme 1). Upon oxidation to a putative $Ta^{I}Au^{I}_2$ trimetallic, the hydride shifts from a broad peak at −1.79 ppm (**2**) to a sharp singlet at +1.45 ppm (**3**). Although this complex has thus far eluded crystallization, the proposed formulation is supported by a full suite of homo- and hetero-nuclear 2D NMR spectroscopies (see ESI† for additional discussion).

A single-electron oxidation of **2** was targeted *via* the addition of one equivalent of FcBArF in thawing DME. Surprisingly, the resultant red-brown product remained diamagnetic; two high-field hydride resonances (−4.33 and −5.33 ppm, each with a relative integration of one proton) were observed in the ^{1}H NMR spectrum. These data are consistent with a one-electron oxidation of **2**, followed by a hydro-

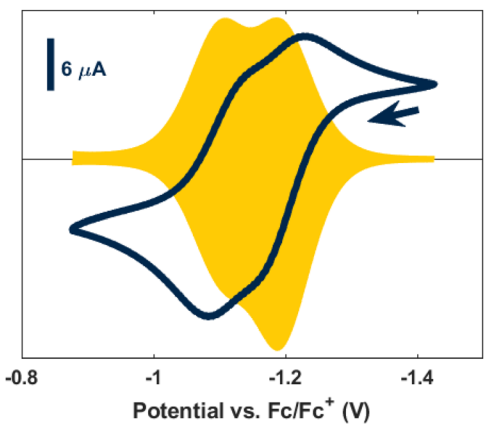

Fig. 4 Cyclic voltammogram (blue) and square wave voltammogram (yellow) of **2**. The tail of the arrow designates the open-circuit potential. The arrowhead indicates the direction of the scan.

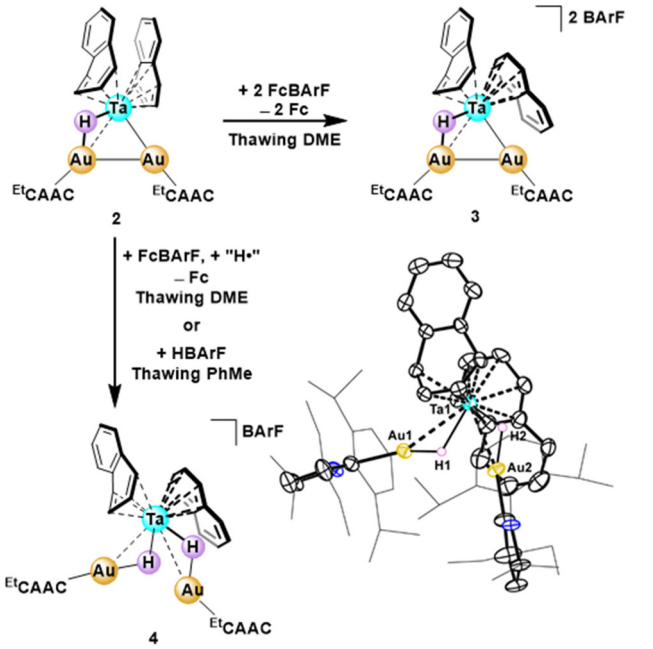

Scheme 1 Either oxidation or protonation of complex **2** affords intact cluster architectures in distinct redox states. The solid-state structure of **4** is shown with thermal anisotropic displacement ellipsoids displayed at the 50% probability level and both non-hydride H-atoms and counterions are omitted for clarity. The hydride H-atoms were resolved in the Fourier map; their locations were refined freely and their U_{iso} values were treated with a riding model.

gen atom abstraction by the open-shell cluster, yielding a formally $Ta^{I}Au^{I}_{2}$ trimetallic dihydride complex $[(^{Et}CAACAu)_2H_2Ta(naph)_2]^+$ (**4**, 36% yield, Scheme 1).[67] Hydrogen atom transfer to the singly oxidized trimetallic is in agreement with the observed electrochemical/chemical behavior in both the SWV and CV of **2** (*vide supra*). To further corroborate the structural identity of **4**, we targeted an independent synthesis through protonation of **2** with Brookhart's acid (HBArF).[68] Addition of one equivalent of HBArF to **2** in thawing toluene produced the same spectral features as the single electron oxidation, further supporting a dihydride cation assignment for **4**.

The structure of **4** was verified through a SCXRD study, in which both hydride ligands were resolved in the Fourier map and refined freely (Scheme 1). Contrasting the core of **2**, **4** features a significantly elongated Au–Au distance of 3.944 Å, expanding to provide room for the second μH ligand. The hydride-supported Ta–Au distances also lengthen upon oxidation to an average of 2.9713(4) Å. However, the average Ta–arene bond distances in **4** (Ta–C_{ave} = 2.366 Å and 2.376 Å, for the η^4 and η^6 naphthyl groups, respectively) are very similar to **1** and **2** (2.348(4)/2.373(4) Å and 2.352(5)/2.411(5) Å for the η^4/η^6 Ta–C_{ave} distances in **1** and **2**, respectively). Correspondingly, naphthalene exchange reactions with myriad substrates across the four multimetallic complexes (**1**–**4**) have thus far proven unsuccessful, either showing no reaction, resulting in intractable decomposition, or forming the bimetallic complex, **1** (Table S1†).

Density functional theory calculations

Whereas oxidation did not render the Ta-bound naphthyl groups labile, the heteromultimetallic series provides a means of exploring the effects of metal identity, redox state, and hydride content on metal–metal bonding. We conducted density functional theory calculations for complexes **1**, $\mathbf{1^{Cu}}$, **2**, **3**, and **4**. The full structures of **1** and $\mathbf{1^{Cu}}$ were optimized at the PBE0-D3(0)/def2-TZVPD level of theory for Ta and Au/Cu, and at the PBE0-D3(0)/def2-SVPD level of theory for all other atoms.[69–72] The full structures of **2**, **3**, and **4** were optimized at the PBE0-D3(0)/def2-SVPD level of theory. In all cases an effective core potential was applied to Ta and Au. Salient DFT findings are summarized in Fig. 5.

The Wiberg bond indices (WBI)[73] for **1** and $\mathbf{1^{Cu}}$ both show Ta-centered M–H bonding, however, the bridging hydrides are more symmetric in the Ta/Au bimetallic. Concomitantly, Natural Population Analysis (NPA) charges and the Ta–M′ WBIs are consistent with greater covalency for the heavier metal pairing. Quantum Theory of Atoms-In-Molecules (QTAIM) analysis[74] shows no Ta–M′ bond critical points, suggesting the bimetallic is supported by 3c2e bonding through the μ_2-hydride. Analysis of the frontier molecular orbitals, which, in spite of the different naphthalene orientations are nearly identical for both the gold and copper congeners, lends additional veracity to the supported nature of the bimetallic core. The HOMOs for each **1** and $\mathbf{1^{Cu}}$ have Ta $5d_{z^2}$ parentage and reflect δ-backbonding into both of the naphthyl

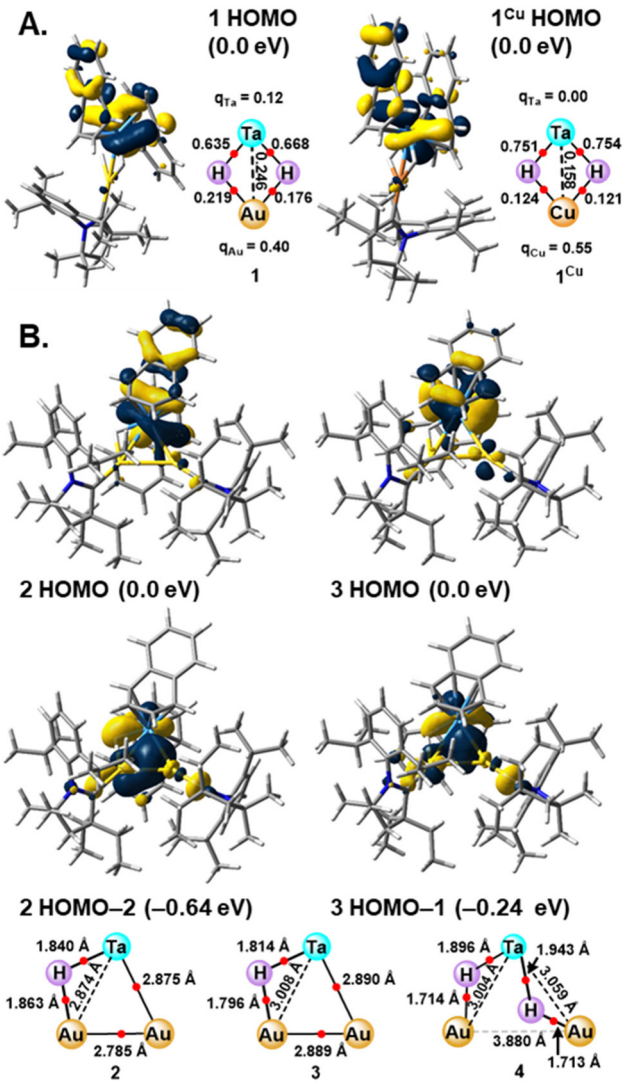

Fig. 5 Calculated HOMOs, Wiberg bond indices, and natural population analysis charges for **1** and $\mathbf{1^{Cu}}$ (A). Select frontier molecular orbitals, as well as select optimized bond metrics, for **2**, **3**, and **4** (B). QTAIM bond critical points are represented by red circles. Orbital isosurfaces are presented at a 0.04 e $Å^{-3}$ level and energies, relative to the HOMO, are provided parenthetically.

rings. Similar Ta–arene interactions dominate the lower energy frontier molecular orbitals (Fig. S35†).

The optimized geometries of **2**, **3**, and **4** were used to inform electronic structure comparisons across the trimetallics, as well as support the locations of the hydride ligands inferred from the SCXRD data. Comparing the structure of **2** to the two-electron oxidized **3** reveals an elongation of the Au–Au and supported Ta–Au distance of approximately 0.1 Å each. Despite this longer Au–Au distance, QTAIM analysis still prescribes a bond critical point between the Au centers. The unsupported Ta–Au bond remains quite similar in both **2** and **3** and likewise displays a bond critical point between the metals. For **2**, the HOMO−2 captures this direct Ta–Au bond, in which a Ta 5d orbital engages in σ-bonding to

the unsupported Au-center (and the μH on the opposite side of the cluster). The Au–Au bonding interaction is likewise clear in the orbital analysis (HOMO−7; Fig. S36†) of **2**. The Ta–Au interaction is present in the HOMO−1 of the oxidized cluster, **3**. In agreement with the weaker Au–Au contact intuited from the bond metrics, no significant orbital overlap is observed between the coinage metals. Consistent with the demonstrated recalcitrance to undergo substitution (*vide infra*), the HOMOs of both **2** and **3** are dominated by Ta–arene backbonding.

The dihydride complex, **4**, is the most structurally distinct trimetallic. Upon protonation, the Au–Au distance increases dramatically (3.880 Å) and the Ta–Au bonds, now both featuring 3c2e hydride bridges, are approximately symmetric. There are no formal M–M bonds in this cluster; QTAIM demonstrates bond critical points exclusively located between M–H interactions. The degradation of direct M–M bonding in **4** is postulated to correlate with experimentally observed instability. Complex **4** decomposes as a solid at room temperature after approximately one week and is only stable in solution at room temperature on the timescale of a few hours. This thermal decomposition leads to intractable mixtures.

The average Ta–arene bond distances for the optimized structures were compared across the five complexes (Table S2†). In agreement with the SCXRD data, no significant difference between Ta–arene bond distances is observed, suggesting that coinage metal identity (Cu *vs.* Au) and cluster charge do not significantly impact Ta–arene bond strength. The HOMOs for all five compounds show significant Ta–arene bonding character, as do lower energy frontier molecular orbitals (*vide supra*). These calculations support the robustness of the Ta–arene interactions, even in the more oxidized structures, as inferred experimentally from the unsuccessful naphthalene exchange experiments.

Arene C–H activation

In an effort to leverage aurophilicity to increase cluster nuclearity,[35,75] trimetallic **2** was treated with one equivalent of both ^{Et}CAACAuCl and NaBArF (a net addition of carbene-supported Au$^+$), affording a dark red solid in 89% yield. The ^{1}H NMR spectrum of this product was consistent with a C_1 symmetric diamagnet featuring two hydrides (δ = −3.16 and −5.89 ppm), three carbenes, and one BArF counter anion. SCXRD revealed the complex as the C–H activated cluster $[(^{Et}CAACAu)_3H_2Ta(C_{10}H_8)(C_{10}H_7)]^+$, **5**, in which the second hydride is sourced from auration of one of the Ta-bound naphthyl rings (Scheme 2). This result highlights the strong Ta–arene interaction, which renders the naphthyl ring prone to functionalization, and recalcitrant to substitution. Moreover, the coinage metal σ-aryl adduct is reminiscent of our previously reported Ta/Cu trimetallic, **Cu$_2$TaHCl** (*cf.* Fig. 2A), in which one copper center activates a naphthalene C–H bond during the initial salt metathesis reaction, and may follow a similar mechanism to related heterobimetallic arene C–H activations reported in the literature.[51,76,77] A comparison of the SCXRD structures of **4** and **5**, which both feature $TaAu_2H_2$ cores, shows little difference in the average Ta–Au distances (2.98 *vs.* 3.06 Å for **4** and **5**, respectively), suggesting that arene substitution has minimal effect on the M–M bonding in the core. A significant discrepancy between the complexes, however, is their solution stability; **5** is stable in THF solution at 40 °C for at least 24 hours. Adding H_2 (1 atm.) at room temperature, however, does impose a transformation, converting **5** to the bimetallic dihydride complex **1**, with concomitant loss of two equivalents of gold. This transformation, though unproductive in terms of accessing higher nuclearity mixed-metal compounds, is analogous to what was observed for closely related **Cu$_2$TaHCl**. Holistically, the strength of the Ta–arene backbonding renders these ligands simultaneously inert to substitution and prone to functionalization, complicating further cluster evolution from these well-defined heteromultimetallic platforms.

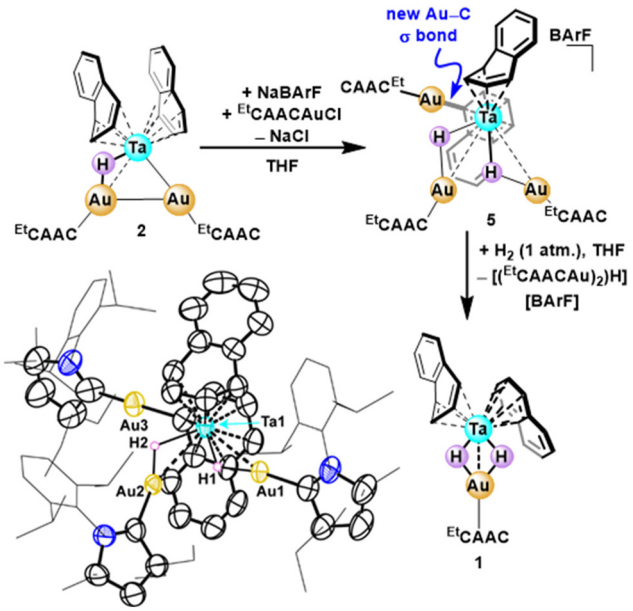

Scheme 2 Synthesis and H_2 reactivity of tetranuclear complex **5**. The solid-state structure of **5** is provided with thermal anisotropic displacement ellipsoids displayed at the 50% probability level. BArF anion and non-hydride H-atoms are omitted for clarity. The hydride H-atoms were resolved in the Fourier map; their locations were refined freely and their U_{iso} values were treated with a riding model.

Conclusions

In summary, we have successfully demonstrated the versatility of arene-supported metalates in metal–metal salt metatheses through the synthesis of rare low-valent Ta/Au heteromultimetallic clusters. Contrasting analogous reactions with copper, carbene-supported gold(I) synthons generate a trimetallic cluster, **2**, upon reaction with $[Ta(naph)_3]^-$. Both SCXRD data and electronic structure calculations corroborate both supported (μH) and unsupported Ta–Au bonding in the trimetallic core. Cluster **2** can activate H_2, but dissociates gold in the process, generating a bimetallic species featuring a Ta–$(\mu H)_2$–

Au core. This compound, adds to the scarce examples of Ta/Au mixed metal complexes, and demonstrates notable structural and reactivity differences in comparison to related Cu analogs. Furthermore, despite the absence of a chelating ancillary ligand framework, trimetallic **2** proves robust, remaining intact through CV-informed chemical oxidation and protonation reactions. Redox chemistry and cluster protonation perturb the Ta–Au bonding, but ultimately seem to have little effect on the lability of the Ta–arene interactions. Further attempts to increase cluster nuclearity highlight the activated nature of the Ta-bound arene rings, resulting in C–H auration *en route* to the tetranuclear dihydride compound **5**. Towards the goal of installing labile ligands on the apical metal center, studies to expand our carbonyl-free salt metathesis protocols to homoleptic polyhydrido metalates are underway in our laboratory.

Author contributions

M. L. M. performed all experiments and DFT calculations, drafted the manuscript, and prepared the ESI.† J. A. B. directed the project, aided in SCXRD refinement, and revised the manuscript/ESI.† Both authors have given approval of the final version of this manuscript.

Data availability

Crystallographic data are available from the Cambridge Structural Database under refcodes 2409547 ($\mathbf{1}^{anti}$), 2409548 (**2**), 2409549 (**4**), 2409550 (**5**), 2432513 ($\mathbf{2}^{SIMes}$), and 2432514 ($\mathbf{LAu(\mu H)AuL}^{+}$).† Full synthetic and computational details, including preparative procedures and spectroscopic data for compound characterization, are available in the ESI.†

Conflicts of interest

There are no conflicts to declare.

Acknowledgements

This work was supported by the University of Michigan and the NSF (Graduate Research Fellowship to M. L. M.—DGE-2241144; XRD Instrumentation—CHE-0840456). We thank Dr Eugenio Alvarado for NMR Spectroscopy expertise and Dr Fengrui Qu and Jeff Kampf are gratefully acknowledged for assistance with SCXRD. Roy Wentz aided in the design and fabrication of glassware that made this work possible.

References

1 M. I. Bruce, B. K. Nicholson, O. B. Shawkataly, J. R. Shapley and T. Henly, Synthesis of Gold-Containing Mixed-Metal Cluster Complexes, in *Inorganic Syntheses*, John Wiley and Sons, 1989, Vol. 26, p 324.

2 P. Braunstein and J. Rose, Gold in Bimetallic Molecular Clusters, *Gold Bull.*, 1985, **18**, 17.

3 E. L. Muetterties, Molecular Metal Clusters, *Science*, 1977, **196**, 839.

4 E. L. Muetterties, T. N. Rhodin, E. Band, C. F. Brucker and W. R. Pretzer, Clusters and Surfaces, *Chem. Rev.*, 1979, **79**, 91.

5 B. Berti, M. Bortoluzzi, C. Cesari, C. Femoni, M. C. Iapalucci, R. Mazzoni and S. Zacchini, A Comparative Experimental and Computational Study of Heterometallic Fe-M (M = Cu, Ag, Au) Carbonyl Clusters Containing N-Heterocyclic Carbene Ligands, *Eur. J. Inorg. Chem.*, 2020, **2020**, 2191.

6 I. Ciabatti, C. Femoni, M. C. Iapalucci, S. Ruggieri and S. Zacchini, The role of gold in transition metal carbonyl clusters, *Coord. Chem. Rev.*, 2018, **355**, 27.

7 O. Lopez-Acevedo, J. Rintala, S. Virtanen, C. Femoni, C. Tiozzo, H. Grönbeck, M. Pettersson and H. Häkkinen, Characterization of Iron−Carbonyl-Protected Gold Clusters, *J. Am. Chem. Soc.*, 2009, **131**, 12573.

8 C. Femoni, M. C. Iapalucci, G. Longoni, C. Tiozzo and S. Zacchini, An Organometallic Approach to Gold Nanoparticles: Synthesis and X-Ray Structure of CO-Protected $Au_{21}Fe_{10}$, $Au_{22}Fe_{12}$, $Au_{28}Fe_{14}$, and $Au_{34}Fe_{14}$ Clusters, *Angew. Chem., Int. Ed.*, 2008, **47**, 6666.

9 N. T. Tran, D. R. Powell and L. F. Dahl, Generation of $AuPd_{22}/Au_2Pd_{21}$ Analogues of the High-Nuclearity $Pd_{23}(CO)_{20}(PEt_3)_{10}$ Cluster Containing 19-atom Centered Hexacapped-Cuboctahedral (ν_2-octahedral) Metal Fragment: Structural-to-Synthesis Approach Concerning Formation of $Au_2Pd_{21}(CO)_{20}(PEt_3)_{10}$, *Dalton Trans.*, 2004, 209.

10 N. T. Tran, D. R. Powell and L. F. Dahl, Nanosized $Au_2Pd_{41}(CO)_{27}(PEt_3)_{15}$ Containing Two Geometrically Unprecedented 13-coordinated Au-centered (μ_{13}-Au)Pd_{13} Polyhedra Connected by Triangular Face-sharing and Three Interpenetrating 12-coordinated Pd-centered (μ_{12}-Pd) Au_2Pd_{10} Icosahedra: Geometrical Change in Centered Polyhedra Induced by Au/Pd Electronegativity-Mismatch, *Dalton Trans.*, 2004, 217.

11 N. T. Tran, M. Kawano, D. R. Powell, R. K. Hayashi, C. F. Campana and L. F. Dahl, Isostructural $[Au_6Pd_6(Pd_{6-x}Ni_x)Ni_{20}(CO)_{44}]^{6-}$ and $[Au_6Ni_{32}(CO)_{44}]^{6-}$ Clusters Containing Corresponding Nonstoichiometric $Au_6Pd_6(Pd_{6-x}Ni_x)Ni_{20}$ and Stoichiometric Au_6Ni_{32} Nanosized Cores: Substitutional Pd/Ni Crystal Disorder (Coloring Problem) at Only Six Specific Nonadjacent Pseudoequivalent Metal Sites in the 38-Atom Trimetallic Close-Packed Framework, *J. Am. Chem. Soc.*, 1999, **121**, 5945.

12 D. M. P. Mingos and M. J. Watson, Heteronuclear Gold Cluster Compounds, in *Advances in Inorganic Chemistry*, ed. A. G. Sykes, Academic Press, 1992, vol. 39, p. 327.

13 A. J. Whoolery and L. F. Dahl, Synthesis and structural-bonding analysis of the $[Au_6Ni_{12}(CO)_{24}]^{2-}$ dianion contain-

ing an unprecedented 18-vertex cubic Td metal core composed of five face-fused octahedra: the first example of a discrete gold/nickel bimetallic-bonded species, *J. Am. Chem. Soc.*, 1991, **113**, 6683.

14 J. E. Ellis, Highly reduced organometallics. 5. Synthesis, properties, and the molecular structure of $(Ph_3PAu)_3V(CO)_5$, a gold-vanadium cluster, *J. Am. Chem. Soc.*, 1981, **103**, 6106.

15 C. E. Coffey, J. Lewis and R. S. Nyholm, 339. Metal–metal bonds. Part I. Compounds of gold(0) with the carbonyls of manganese, iron, and cobalt, *J. Chem. Soc.*, 1964, 1741.

16 B. C. Gates, Extending the Metal Cluster–Metal Surface Analogy, *Angew. Chem., Int. Ed. Engl.*, 1993, **32**, 228.

17 G. Ertl, Chapter 11 Relations Between Metal Clusters and Metal Surfaces, in *Studies in Surface Science and Catalysis*, ed. B. C. Gates, L. Guczi and H. Knozinger, Elsevier, 1986, vol. 29, p. 577.

18 M. Moskovits, Metal cluster complexes and heterogeneous catalysis - a heterodox view, *Acc. Chem. Res.*, 1979, **12**, 229.

19 H. S. Taylor and E. F. Armstrong, A theory of the catalytic surface, *Proc. R. Soc. London*, 1997, **108**, 105.

20 G. A. Somorjai, Surface Science and Catalysis, *Science*, 1985, **227**, 902.

21 M. Landrini, M. Navarro, J. Campos and L. Rocchigiani, Enhanced reactivity of cationic $Au(\mu\text{-}H)_2MCp_2$ complexes (M = Mo and W) enabled by bulky tris-biaryl phosphines, *Dalton Trans.*, 2025, **54**, 898.

22 A. Lachguar, I. Del Rosal, L. Maron, E. Jeanneau, L. Veyre, C. Thieuleux and C. Camp, π-Bonding of Group 11 Metals to a Tantalum Alkylidyne Alkyl Complex Promotes Unusual Tautomerism to Bis-alkylidene and CO_2 to Ketenyl Transformation, *J. Am. Chem. Soc.*, 2024, **146**, 18306.

23 M. Landrini, R. Patel, J. Tyrrell-Thrower, A. Macchioni, D. L. Hughes, L. Tensi, P. Hrobárik and L. Rocchigiani, Exploring Ligand Effects on Structure, Bonding, and Photolytic Hydride Transfer of Cationic Gold(I) Bridging Hydride Complexes of Molybdocene and Tungstenocene, *Inorg. Chem.*, 2024, **63**, 13525.

24 L. Rocchigiani, W. T. Klooster, S. J. Coles, D. L. Hughes, P. Hrobárik and M. Bochmann, Hydride Transfer to Gold: Yes or No? Exploring the Unexpected Versatility of Au···H–M Bonding in Heterobimetallic Dihydrides, *Chem. – Eur. J.*, 2020, **26**, 8267.

25 N. P. Mankad, Diverse bimetallic mechanisms emerging from transition metal Lewis acid/base pairs: development of co-catalysis with metal carbenes and metal carbonyl anions, *Chem. Commun.*, 2018, **54**, 1291.

26 A. Hicken, A. J. P. White and M. R. Crimmin, Selective Reduction of CO_2 to a Formate Equivalent with Heterobimetallic Gold–-Copper Hydride Complexes, *Angew. Chem., Int. Ed.*, 2017, **56**, 15127.

27 M. K. Karunananda, S. R. Parmelee, G. W. Waldhart and N. P. Mankad, Experimental and Computational Characterization of the Transition State for C–X Bimetallic Oxidative Addition at a Cu–Fe Reaction Center, *Organometallics*, 2015, **34**, 3857.

28 P. Buchwalter, J. Rosé and P. Braunstein, Multimetallic Catalysis Based on Heterometallic Complexes and Clusters, *Chem. Rev.*, 2015, **115**, 28.

29 A. Albinati and L. M. Venanzi, Transition metal hydrides as ligands, *Coord. Chem. Rev.*, 2000, **200–202**, 687.

30 L. H. Pignolet, M. A. Aubart, K. L. Craighead, R. A. T. Gould, D. A. Krogstad and J. S. Wiley, Phosphine-stabilized, platinum-gold and palladium-gold cluster compounds and applications in catalysis, *Coord. Chem. Rev.*, 1995, **143**, 219.

31 A. Antiñolo, F. A. Jalón, A. Otero, M. Fajardo, B. Chaudret, F. Lahoz and J. A. López, Reactivity of ruthenium and niobium trihydrides with gold fragments. Crystal structure of the hexanuclear raft cluster $[Au_3Nb_3(\mu\text{-}H)_6(\eta\text{-}C_5H_4SiMe_3)_6]$, *J. Chem. Soc., Dalton Trans.*, 1991, 1861.

32 B. D. Alexander, M. P. Gomez-Sal, P. R. Gannon, C. A. Blaine, P. D. Boyle, A. M. Mueting and L. H. Pignolet, Heterobimetallic gold-osmium and gold-ruthenium hydrido complexes. X-ray crystal and molecular structures of $[Au_2Os(H)_3(PPh_3)_5]PF_6$ and $[AuRu(H)_2(CO)(PPh_3)_4]PF_6$, *Inorg. Chem.*, 1988, **27**, 3301.

33 B. D. Alexander, B. J. Johnson, S. M. Johnson, P. D. Boyle, N. C. Kann, A. M. Mueting and L. H. Pignolet, Heterobimetallic gold-iridium, silver-iridium, and gold-ruthenium bis(μ-hydrido) complexes. X-ray crystal and molecular structures of $[AuRu(H)_2(dppm)_2(PPh_3)]PF_6$ and $[Ir(H)_2(bpy)(PPh_3)_2]PF_6$, *Inorg. Chem.*, 1987, **26**, 3506.

34 B. R. Sutherland, K. Folting, W. E. Streib, D. M. Ho, J. C. Huffman and K. G. Caulton, Synthetic and mechanistic features of alcohol elimination between gold alkoxides and rhenium polyhydrides. Metal polyhedron reconstruction upon protonation, *J. Am. Chem. Soc.*, 1987, **109**, 3489.

35 M. Fajardo, M. P. Gómez-Sal, P. Royo, S. Martínez Carrera and S. García Blanco, Synthesis and structural characterisation of the mixed-metal cluster cation $[Nb(\eta^5\text{-}C_5H_4R)_2\{AuP(C_6H_5)_3\}_2]^+$ with R = H or $Si(CH_3)_3$, *J. Organomet. Chem.*, 1986, **312**, C44.

36 H. Lehner, D. Matt, P. S. Pregosin, L. M. Venanzi and A. Albinati, Stable gold hydride complexes, *J. Am. Chem. Soc.*, 1982, **104**, 6825.

37 M. A. Gawish, Q. A. Drmosh and S. A. Onaizi, Single Atom Catalysts: An Overview of the Coordination and Interactions with Metallic Supports, *Chem. Rec.*, 2022, **22**, e202100328.

38 X. Y. Liu, A. Wang, T. Zhang and C.-Y. Mou, Catalysis by gold: New insights into the support effect, *Nano Today*, 2013, **8**, 403.

39 J. A. Rodriguez, S. D. Senanayake, D. Stacchiola, P. Liu and J. Hrbek, The Activation of Gold and the Water–Gas Shift Reaction: Insights from Studies with Model Catalysts, *Acc. Chem. Res.*, 2014, **47**, 773.

40 B. Hammer and J. K. Norskov, Why gold is the noblest of all the metals, *Nature*, 1995, **376**, 238.

41 J. Schwank, Gold in bimetallic catalysts, *Gold Bull.*, 1985, **18**, 2.

42 A. Mahdavi-Shakib, T. N. Whittaker, T. Y. Yun, K. B. Sravan Kumar, L. C. Rich, S. Wang, R. M. Rioux, L. C. Grabow and B. D. Chandler, The role of surface hydroxyls in the entropy-driven adsorption and spillover of H_2 on Au/TiO_2 catalysts, *Nat. Catal.*, 2023, **6**, 710.

43 R. Guo, X. Xu, Y. Xia, W. Huang, Z. Li and B. Teng, , Insights into electrocatalytic hydrogen evolution reaction in acidic medium at *in situ* dispersed Pt atoms on nanoporous gold films, *J. Catal.*, 2018, **368**, 379.

44 J. Cornejo-Romero, A. Solis-Garcia, S. M. Vega-Diaz and J. C. Fierro-Gonzalez, Reverse hydrogen spillover during ethanol dehydrogenation on TiO_2-supported gold catalysts, *Mol. Catal.*, 2017, **433**, 391.

45 P. Schlexer and G. Pacchioni, Anchoring Small Au Clusters on the Dehydroxylated and Hydroxylated SiO_2 α-Quartz (001) Surface via Ti-Alloying, *J. Phys. Chem. C*, 2017, **121**, 14717.

46 D. Nabaho, J. W. Niemantsverdriet, M. Claeys and E. v. Steen, Hydrogen spillover in the Fischer–Tropsch synthesis: An analysis of gold as a promoter for cobalt–alumina catalysts, *Catal. Today*, 2016, **275**, 27.

47 S. S. E. Collins, M. Cittadini, C. Pecharromán, A. Martucci and P. Mulvaney, Hydrogen Spillover between Single Gold Nanorods and Metal Oxide Supports: A Surface Plasmon Spectroscopy Study, *ACS Nano*, 2015, **9**, 7846.

48 J. Campos, Bimetallic cooperation across the periodic table, *Nat. Rev. Chem.*, 2020, **4**, 696.

49 A. W. Beamer and J. A. Buss, Surface-like NO_x Reduction at an Atomically-Precise Tricopper Cluster, *Angew. Chem., Int. Ed.*, 2025, e202424772.

50 A. W. Beamer and J. A. Buss, Synthesis, Structural Characterization, and CO_2 Reactivity of a Constitutionally Analogous Series of Tricopper Mono-, Di-, and Trihydrides, *J. Am. Chem. Soc.*, 2023, **145**, 12911.

51 M. L. Maiola and J. A. Buss, Accessing Ta/Cu Architectures via Metal-Metal Salt Metatheses: Heterobimetallic C–H Bond Activation Affords μ-Hydrides, *Angew. Chem., Int. Ed.*, 2023, **62**, e202311721.

52 W. W. Brennessel, J. E. Ellis, M. K. Pomije, V. J. Sussman, E. Urnezius and V. G. Young, Tris(η^4-naphthalene)- and Tris(1–4-η^4-anthracene)tantalate(1−): First Homoleptic Arene Complexes of Anionic Tantalum, *J. Am. Chem. Soc.*, 2002, **124**, 10258.

53 A. S. Romanov, C. R. Becker, C. E. James, D. Di, D. Credgington, M. Linnolahti and M. Bochmann, Copper and Gold Cyclic (Alkyl)(amino)carbene Complexes with Sub-Microsecond Photoemissions: Structure and Substituent Effects on Redox and Luminescent Properties, *Chem. – Eur. J.*, 2017, **23**, 4625.

54 In our previously reported Cu/Ta system (see ref. 51), we found that the reducing reaction conditions promoted C–H activation of the naphthalene rings and HAT from solvent, resulting in the incorporation of hydride ligands. H/D scrambling in the gold system prevents such precise isotopic labeling experiments; reactions from either [Ta(naph-d_8)$_3$]$^-$ or those run in THF-d_8 result in partial deuterium incorporation in **2**. In light of the multi-step reaction sequence involved in generating **2**, the low reaction yield, and the scrambling observed in attempts to label the hydride, we hesitate to speculate as to the exact balance of this reaction.

55 K. Chakarawet, Z. W. Davis-Gilbert, S. R. Harstad, V. G. Young Jr, J. R. Long and J. E. Ellis, Ta(CNDipp)$_6$: An Isocyanide Analogue of Hexacarbonyltantalum(0), *Angew. Chem., Int. Ed.*, 2017, **56**, 10577.

56 F. A. Cotton, C. A. Murillo and R. A. Walton, *Multiple Bonds Between Metal Atoms. 3rd ed*, Springer, New York, 2005.

57 The formal oxidation state assignments in cluster **2** are ambiguous. We favor $Ta^{-I}Au^{I}Au^{I}$; however, another reasonable assignment invokes a antiferromagnetically coupled $Ta^{0}Au^{I}Au^{0}$ core, where the oxidized Au center bears the bridging hydride. Efforts to inform the formal oxidation state at Ta *via* Ta–arene bond metrics were unsuccessful (see Tables S2 & S4; additional discussion is presented in the ESI†).

58 J. D. Lee, Z. Qi, A. C. Foucher, H. T. Ngan, K. Dennis, J. Cui, I. I. Sadykov, E. J. Crumlin, P. Sautet, E. A. Stach, C. M. Friend, R. J. Madix and J. Biener, Facilitating Hydrogen Dissociation over Dilute Nanoporous Ti–Cu Catalysts, *J. Am. Chem. Soc.*, 2022, **144**, 16778.

59 R. Réocreux, E. C. H. Sykes, A. Michaelides and M. Stamatakis, Stick or Spill? Scaling Relationships for the Binding Energies of Adsorbates on Single-Atom Alloy Catalysts, *J. Phys. Chem. Lett.*, 2022, **13**, 7314.

60 J. E. S. van der Hoeven, H. T. Ngan, A. Taylor, N. M. Eagan, J. Aizenberg, P. Sautet, R. J. Madix and C. M. Friend, Entropic Control of HD Exchange Rates over Dilute Pd-in-Au Alloy Nanoparticle Catalysts, *ACS Catal.*, 2021, **11**, 6971.

61 F. R. Lucci, M. D. Marcinkowski, T. J. Lawton and E. C. H. Sykes, H_2 Activation and Spillover on Catalytically Relevant Pt–Cu Single Atom Alloys, *J. Phys. Chem. C*, 2015, **119**, 24351.

62 F. R. Lucci, J. Liu, M. D. Marcinkowski, M. Yang, L. F. Allard, M. Flytzani-Stephanopoulos and E. C. H. Sykes, Selective hydrogenation of 1,3-butadiene on platinum–copper alloys at the single-atom limit, *Nat. Commun.*, 2015, **6**, 8550.

63 G. Kyriakou, M. B. Boucher, A. D. Jewell, E. A. Lewis, T. J. Lawton, A. E. Baber, H. L. Tierney, M. Flytzani-Stephanopoulos and E. C. H. Sykes, Isolated Metal Atom Geometries as a Strategy for Selective Heterogeneous Hydrogenations, *Science*, 2012, **335**, 1209.

64 Partial decomposition to unknown hydride/deuteride containing byproducts is observed concomitantly with the conversion of $\mathbf{1^H}$ to $\mathbf{1^D}$; however, ^{1}H NMR signals corresponding to the carbene ligand of **1** support it is the major species in solution following treatment of $\mathbf{1^H}$ with D_2 gas (see Fig. S27).†

65 V. J. Sussman and J. E. Ellis, From Storable Sources of Atomic Nb− and Ta− Ions to Isolable Anionic Tris(1,3-butadiene)metal Complexes: [M(η^4-C_4H_6)$_3$]$^-$, M=Nb, Ta, *Angew. Chem., Int. Ed.*, 2008, **47**, 484.

66 N. Elgrishi, K. J. Rountree, B. D. McCarthy, E. S. Rountree, T. T. Eisenhart and J. L. Dempsey, A Practical Beginner's Guide to Cyclic Voltammetry, *J. Chem. Educ.*, 2018, **95**, 197.

67 We have repeated the single electron oxidation of **2** in DME-d_{10}; however, no deuterium is incorporated into the product, **4**.

68 M. Brookhart, B. Grant and A. F. Volpe, Jr., [(3,5-$(CF_3)_2C_6H_3)_4B]^-[H(OEt_2)_2]^+$: a convenient reagent for generation and stabilization of cationic, highly electrophilic organometallic complexes, *Organometallics*, 1992, **11**, 3920.

69 S. Grimme, J. Antony, S. Ehrlich and H. Krieg, A consistent and accurate ab initio parametrization of density functional dispersion correction (DFT-D) for the 94 elements H-Pu, *J. Chem. Phys.*, 2010, **132**, 154104.

70 F. Weigend and R. Ahlrichs, Balanced basis sets of split valence, triple zeta valence and quadruple zeta valence quality for H to Rn: Design and assessment of accuracy, *Phys. Chem. Chem. Phys.*, 2005, **7**, 3297.

71 C. Adamo and V. Barone, Toward reliable density functional methods without adjustable parameters: The PBE0 model, *J. Chem. Phys.*, 1999, **110**, 6158.

72 D. Andrae, U. Huermann, M. Dolg, H. Stoll and H. L. Preu, Energy-adjustedab initio pseudopotentials for the second and third row transition elements, *Theor. Chim. Acta*, 1990, **77**, 123.

73 K. B. Wiberg, Application of the pople-santry-segal CNDO method to the cyclopropylcarbinyl and cyclobutyl cation and to bicyclobutane, *Tetrahedron*, 1968, **24**, 1083.

74 T. Lu and F. Chen, Multiwfn: A multifunctional wavefunction analyzer, *J. Comput. Chem.*, 2012, **33**, 580.

75 E. Y. Tsui, P. Müller and J. P. Sadighi, Reactions of a Stable Monomeric Gold(I) Hydride Complex, *Angew. Chem., Int. Ed.*, 2008, **47**, 8937.

76 I. Del Rosal, S. Lassalle, C. Dinoi, C. Thieuleux, L. Maron and C. Camp, Mechanistic investigations via DFT support the cooperative heterobimetallic C–H and O–H bond activation across Ta=Ir multiple bonds, *Dalton Trans.*, 2021, **50**, 504.

77 M. G. Alférez, J. J. Moreno, N. Hidalgo and J. Campos, Reversible Hydride Migration from C_5Me_5 to RhI Revealed by a Cooperative Bimetallic Approach, *Angew. Chem., Int. Ed.*, 2020, **59**, 20863.